axioms

MDPI

Article

Predicting Sit-to-Stand Body Adaptation Using a Simple Model

Sarra Gismelseed *, Amur Al-Yahmedi, Riadh Zaier, Hassen Ouakad and Issam Bahadur

Department of Mechanical & Industrial Engineering, College of Engineering, Sultan Qaboos University, Muscat 123, Oman; amery@squ.edu.om (A.A.-Y.); zaier@squ.edu.om (R.Z.); houakad@squ.edu.om (H.O.); bahdoor@squ.edu.om (I.B.)

* Correspondence: sarraabbasher@gmail.com

Abstract: Mathematical models that simulate human motion are used widely due to their potential in predicting basic characteristics of human motion. These models have been involved in investigating various aspects of gait and human-related tasks, especially walking and running. This study uses a simple model to study the impact of different factors on sit-to-stand motion through the formulation of an optimization problem that aims at minimizing joint torques. The simulated results validated experimental results reported in the literature and showed the ability of the model to predict the changes in kinetic and kinematic parameters as adaptation to any change in the speed of motion, reduction in the joint strength, and change in the seat height. The model discovered that changing one of these determinants would affect joint angular displacement, joint torques, joint angular velocities, center of mass position, and ground reaction force.

Keywords: sit-to-stand; discrete mechanics; optimization; sit-to-stand determinates

MSC: 37N99

check for updates

Citation: Gismelseed, S.; Al-Yahmedi, A.; Zaier, R.; Ouakad, H.; Bahadur, I. Predicting Sit-to-Stand Body Adaptation Using a Simple Model. *Axioms* **2023**, *12*, 559. https://doi.org/10.3390/axioms12060559

Academic Editors: Siamak Pedrammehr and Mohammad Reza Chalak Qazani

Received: 14 April 2023
Revised: 25 May 2023
Accepted: 31 May 2023
Published: 5 June 2023

Copyright: © 2023 by the authors. Licensee MDPI, Basel, Switzerland. This article is an open access article distributed under the terms and conditions of the Creative Commons Attribution (CC BY) license (https://creativecommons.org/licenses/by/4.0/).

1. Introduction

Mathematical models that simulate human motion and capture the basic pattern of human motor characteristics in the absence of empirical data (or what is known as predictive simulation [1]), were used to study many human kinetic characteristics, such as targeting a specific kinetic speed while reducing the metabolic cost associated with this movement [1,2]. By applying dynamic optimization processes while considering physical and physiological constraints [3,4], researchers were able to derive whole body dynamics, aiding in the production of movements that closely resemble human motion by controlling relevant parameters. Most of the predictive simulation studies were done to study human gait characteristics since it is the main feature of human beings [3,5,6]; however, Sit-to-Stand (STS) motion is also one of the main daily activities, which is also considered as a distinctive feature of human beings.

STS motion has been attracting scientists and physical therapists to experimentally study and analyze the aspects of how humans perform this task that is mainly defined by the process of going to a standing position from a sitting position [7,8]. This motion has a direct effect on humans' quality of life, and the significance of this motion will not be appreciated until it becomes physically or cognitively challenging, which can be temporary due to injury or permanent due to aging or illness. All the previous reasons may cause difficulties in completing this motion successfully, especially in an elderly population. Studies showed that at the age of 55 years and above, 45% of women and 30% of men suffer from moderate to serious inabilities in rising from sitting [9]. Inability to properly perform the STS motion may be associated with decreased mobility and balance, with an increased risk of falling, as well. Several factors influencing the performance of STS motion are considered as determinants, as they can either facilitate successful completion of the task or make it more challenging [10,11]. The determinants of STS motion have

been categorized into different groups according to the source of the determinates, which are strategy-related determinants such as speed, foot position, trunk rotation, etc. [8,11]; subject-related determinants such as age, muscle force, and disease [7,12,13]; and chair-related determinants [14,15] such as seat height, armrests, and backrest [16,17]. The impact of these determinants on body behavior and movement performance differs according to the type of determinants, and it has been studied in order to investigate how the body adapts to the changes of these determinants.

The predictive simulation has been involved in studying the STS motion [6,18] to have a better understanding of how we usually move and when this movement occurs [18]. A good understanding of the normal way of movement during STS will help as well in applying this knowledge to some cases of predictive simulation that involve studying losing mobility or some difficulties in performing this task. The complexity of biomechanical models used to study STS motion varies from simple to complicated based on the number of segments and muscles included in these models, in addition to the number of planes used in the modeling [9,19]. Most of the models were modeled as 2D models in the sagittal plane [20] since most of the joints' movement occur in this plane; however, few were modeled as 3D models. These models were involved in studying various aspects of STS motion and the effect of different parameters on this motion, including the effect of chair height, the effect of initial foot position, the effect of muscle strength, etc. Garner proposed a biomechanical model modeled in the sagittal plane that has three rigid segments (i.e., thigh, leg, and HAT (Head, Arms, and Torso) and eight muscles [19]. Garner used dynamic optimization to explain the execution of this motion by minimizing a cost function split into two parts; the first part is aimed at minimizing muscle stress until the time the biped leaves the chair, and the second part is aimed at minimizing peak forces developed by the muscles from the time the biped leaves the chair until the time required to accomplish this task [19]. This cost function produced simulation results that were very similar to the experimental results. The model of Garner is further enhanced by Daigle by adding a foot segment and increasing the number of muscles to 18 [20], and the model was used to understand the difficulties related to muscle strength and its effect on accomplishing this task by using an optimization formulation that minimizes the motion time with different muscle strength varied from 50% to 200% [20]. The model was able to define which muscles have a great contribution and power activation in the sit-to-stand task [20]. On other hand, Domire used a sagittal plane model that consists of three links connected with three joints and actuated by eight muscles to study the effect of seat height on STS motion [21]. Domire predicted the effect of seat height using the same objective function described by Garner and simulated the movement during STS from different seat heights, adjusted by rotating the thigh segment at four different angles: 80°, 90°, 98°, and 100° [21]. The study concluded that as the seat height decreased, the movement of STS became more difficult, and it was impossible at the lowest seat height corresponding to the 100° thigh angle.

In this study, a simple 2D model is used to predict the effect of changing three STS determinants (speed, joint strength, and seat height) on lower limb and upper body kinetic and kinematic parameters by applying dynamic optimization to minimize the joint torques. First, the derivation of the proposed model and the formulation of the optimization problem are shown in the following section. Then, the simulation results are shown in the third section of this study with the validation of some simulation results with experimental results from the literature. In the fourth section, results from this study are discussed and compared to reported results and conclusions from experimental studies. Finally, we summarize our work with the main conclusions in the last section.

2. Materials and Methods

Accurately predicting STS motion requires a biomechanics model that accurately represents the human body, as well as an understanding of how to identify the specific movements involved in STS motion. The model proposed in this study is modeled in the sagittal plane since the movement of humans' joints are mostly obvious when it is seen

from the sagittal plane compared to the other planes [22]. This will allow for simplifying the human body to a three-links model, as shown in Figure 1, through assuming that the two legs are symmetrical and can be modeled as one leg with two segments, tibia and femur, in addition to the torso segment. A male subject of height 1.70 m and mass 70 kg is considered for approximating the model physical parameters. The physical parameters shown in Table 1 were calculated using anthropometric percentages compiled by different investigators (the detailed calculations are given in Appendix A) [23–25].

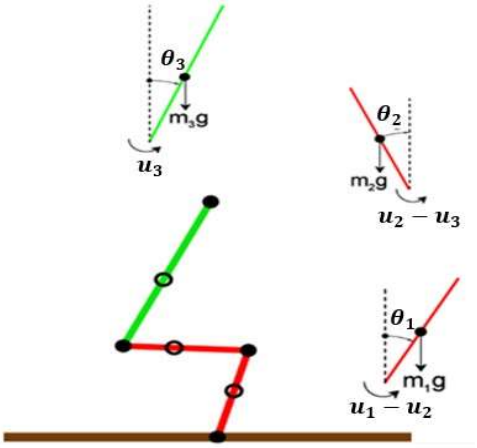


Figure 1. Three-links model, u_i is the torque applied at each joint, and each link is assigned with a number: 1 = stance tibia, 2 = stance femur, 3 = trunk.

Table 1. Physical parameters.

Link	Body Segment	Length of Segment (m) l_i	Distance from Center of Mass to Next Joint (m) d_i	Mass of Segment (kg) m_i	Moment of Inertia of Segment (kg·m^2) I_i
1	tibia	0.390	0.182	6.650	0.088
2	femur	0.420	0.170	14.70	0.163
3	torso	0.690	0.372	46.60	2.068

The problem is formulated as an optimization problem in the goal is to minimize a given cost function while satisfying constraints imposed by the task. Due to the high degree of nonlinearity of the problem, the use of the direct (single) shooting method to solve the resulting optimization problem may likely cause the algorithm to fail to find a solution. One can either use collocation methods or use direct discretization of the Lagrange-d'Alembert Principle for the system. We chose to use direct discretization of the Lagrange-d'Alembert Principle (discrete mechanics) [26,27]. Discrete mechanics requires that the Lagrange equation of the system be derived first. The Lagrange equation of the model is given by:

$$\begin{aligned}\mathcal{L} = \tfrac{1}{2}\Big(m_1(l_1-d_1)^2 \quad & +m_2l_1^2+m_3l_1^2)\dot{\theta}_1^2+\tfrac{1}{2}\Big(m_2(l_2-d_2)^2+m_3l_2^2\Big)\dot{\theta}_2^2+\tfrac{1}{2}m_3d_3^2\dot{\theta}_3^2\\ & -(m_2l_1(l_2-d_2)+m_3l_1l_2)\dot{\theta}_1\dot{\theta}_2cos(\theta_1+\theta_2)+m_3l_1d_3\dot{\theta}_1\dot{\theta}_3cos(\theta_1-\theta_3)\\ & -m_3l_2d_3\dot{\theta}_2\dot{\theta}_3cos(\theta_2+\theta_3)-g(m_1(l_1-d_1)+m_2l_1+m_3l_1)cos\theta_1\\ & -g(m_2(l_2-d_2)+m_3l_2)cos\theta_2-m_3gd_3cos\theta_3\end{aligned} \tag{1}$$

the discrete Lagrange equation is derived from the continuous Lagrange equation, using the mid-point rule as follows (for the detailed derivations, check Appendix A):

$$\mathcal{L}(q,\dot{q}) \rightarrow h\mathcal{L}_d\left(\frac{q_{k+1}+q_k}{2},\frac{q_{k+1}-q_k}{h}\right) \tag{2}$$

The system dynamics is then:

$$\begin{aligned} D_1\mathcal{L}_d(\theta_{1k},\theta_{1k+1}, \quad & \theta_{2k},\theta_{2k+1},\theta_{3k},\theta_{3k+1}) + {f_d}^-(\theta_{1k},\theta_{1k+1},\theta_{2k},\theta_{2k+1},\theta_{3k},\theta_{3k+1}) \\ & + D_2\mathcal{L}_d(\theta_{1k-1},\theta_{1k},\theta_{2k-1},\theta_{2k},\theta_{3k-1},\theta_{3k}) \\ & + {f_d}^+(\theta_{1k-1},\theta_{1k},\theta_{2k-1},\theta_{2k},\theta_{3k-1},\theta_{3k}) = 0 \end{aligned} \tag{3}$$

where $D_1\mathcal{L}_d(\theta_{1k},\theta_{1k+1},\theta_{2k},\theta_{2k+1},\theta_{3k},\theta_{3k+1})$ is the first derivative of the discrete Lagrange with respect to current coordinates (i.e., θ_{1k}, θ_{2k}, and θ_{3k}), and is the first derivative of the discrete Lagrange with respect to future coordinates (i.e., $\theta_{1k+1}, \theta_{2k+1}$, and θ_{3k+1}).

$$D_1\mathcal{L}_d = \begin{bmatrix} \frac{\partial \mathcal{L}_d}{\partial \theta_{1k}}(\theta_{1k},\theta_{1k+1},\theta_{2k},\theta_{2k+1},\theta_{3k},\theta_{3k+1}) \\ \frac{\partial \mathcal{L}_d}{\partial \theta_{2k}}(\theta_{1k},\theta_{1k+1},\theta_{2k},\theta_{2k+1},\theta_{3k},\theta_{3k+1}) \\ \frac{\partial \mathcal{L}_d}{\partial \theta_{3k}}(\theta_{1k},\theta_{1k+1},\theta_{2k},\theta_{2k+1},\theta_{3k},\theta_{3k+1}) \end{bmatrix} \tag{4}$$

$$D_2\mathcal{L}_d = \begin{bmatrix} \frac{\partial \mathcal{L}_d}{\partial \theta_{1k+1}}(\theta_{1k},\theta_{1k+1},\theta_{2k},\theta_{2k+1},\theta_{3k},\theta_{3k+1}) \\ \frac{\partial \mathcal{L}_d}{\partial \theta_{2k+1}}(\theta_{1k},\theta_{1k+1},\theta_{2k},\theta_{2k+1},\theta_{3k},\theta_{3k+1}) \\ \frac{\partial \mathcal{L}_d}{\partial \theta_{3k+1}}(\theta_{1k},\theta_{1k+1},\theta_{2k},\theta_{2k+1},\theta_{3k},\theta_{3k+1}) \end{bmatrix} \tag{5}$$

Both discrete torques, i.e., left and right forces, are defined as follows.

$${u_d}^- = {u_d}^+ = \begin{bmatrix} u_{1k} - u_{2k} \\ u_{2k} - u_{3k} \\ u_{3k} \end{bmatrix} \tag{6}$$

To raise the body from the sitting position to the standing position, it is necessary to provide an appropriate amount of torque at the joints. Therefore, an optimization problem is formulated to mimic the Sit-to-Stand function with the aim of minimizing the effort required to complete this motion, which is represented as the total torque-squared applied by each joint [28]. The torques are equally minimized ($\alpha_1 = \alpha_2 = \alpha_3 = 1$) to study the effect of speed and seat height on the motion; however, α_2 (coefficient of the knee torque) is increased to study the effect of knee strength while keeping $\alpha_1 = \alpha_3 = 1$, assuming that the model is mimicking sitting on a desk chair in which the femur is making a 90° angle with the vertical axis, whereas the tibias and torso are allowed to have unfixed initial states but within reasonable bounded range. Conversely, the standing position requires all joints to make around 0° with the vertical as defined in our model. Then, the optimization problem can be simplified as follows:

$$\min J = \sum_{k=1}^{N}\sum_{i=1}^{3} \alpha_i {u_i}^2(N) = \sum_{k=1}^{N} \alpha_1 u_1^2(N) + \alpha_2 u_2^2(N) + \alpha_3 u_3^2(N) \tag{7}$$

with both decision variables θ_i and u_i subjected to the following constraints:

- System dynamics

$$\begin{aligned} D_1\mathcal{L}_d(\theta_{1k},\theta_{1k+1}, \quad & \theta_{2k},\theta_{2k+1},\theta_{3k},\theta_{3k+1}) + {f_d}^-(\theta_{1k},\theta_{1k+1},\theta_{2k},\theta_{2k+1},\theta_{3k},\theta_{3k+1}) \\ & + D_2\mathcal{L}_d(\theta_{1k-1},\theta_{1k},\theta_{2k-1},\theta_{2k},\theta_{3k-1},\theta_{3k}) \\ & + {f_d}^+(\theta_{1k-1},\theta_{1k},\theta_{2k-1},\theta_{2k},\theta_{3k-1},\theta_{3k}) = 0 \end{aligned}$$

- Boundary constraints

$$\theta_3(1) = 0^\circ, \theta_2(1) = 90^\circ$$

$$\theta_1(N+1) = 0^\circ, \theta_2(N+1) = 0^\circ, \theta_3(N+1) = 0^\circ$$

- Path constraints

$$\theta_{i\ min} \leq \theta_i \leq \theta_{i\ max}$$

$$u_{i\ min} \leq u_i \leq u_{i\ max}$$

The optimization problem was solved using the MATLAB® and SNOPT® (Sparse Nonlinear OPTimizer) toolbox, and the simulation was run with different initial conditions for each case in this study.

3. Results

The results of the optimization provided a unique solution for each case that describes the optimal STS movement for the given conditions. The normal pattern of STS can be explained using the ground force and the velocity of Center of Mass (COM) by dividing the STS motion into phases, starting from the model at sitting position and ending when the velocity of center of mass approaches zero [29]. The first phase starts at the sitting position and initiates the movement by bending the torso forward, and it ends by raising both thighs, as seen in Figure 2. Bending the torso forward helps to get torso flexion, which shifts COM forward. This phase transfers momentum to the next phase, and it occurs quickly. Therefore, it requires the generation of an efficient flexion momentum to be able to transfer a lot of it to the lower extremities in the next phase. Before standing up, the tibia segment is placed backward behind the knee, which results in ankle dorsiflexion. The results showed that the profile of GRF directed forward under the feet and the velocity of COM have a bell shape with a peak just before seat off, as seen in Figures 3 and 4 respectively [29]. The GRF for the model and the experimental results [30] have the same pattern; however, for the case of the experimental results, the GRF starts from zero due to the presence of the chair that holds the weight of the person. For the model, the GRF as a percentage of body weight starts from one because we assume that the model is at the sitting position on foot (no chair). Moreover, we noticed that the model obtained the same profile of COM velocity reported in the literature [29].

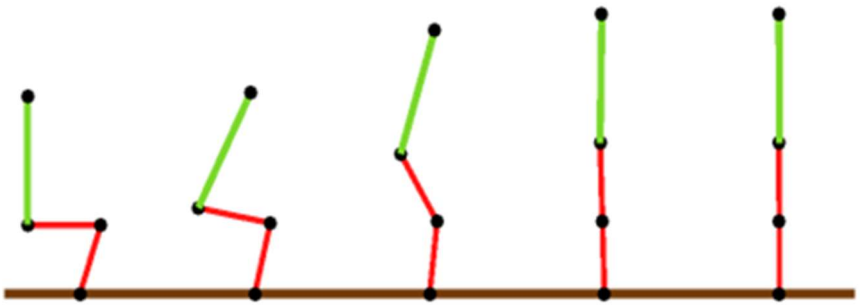


Figure 2. The normal pattern of STS can be explained using the ground force reaction and the velocity of center of mass by dividing the movement into phases starting from the model sitting and ending when the velocity of center of mass approaches zero.

Then, the model is considered to be in the second phase once it is no longer in the sitting position. The hip will continue to flex, and the model uses the flexion momentum transferred from the previous phase, which was generated from torso flexion and distributed to all segments, but more to the lower segments. For human beings, the flexion momentum produced in the first phase is for the upper body, since the thighs are still on the seat. Whenever the thighs are taken off the seat, this flexion momentum can be transferred to the total body and into the legs, as well. Meanwhile, we will have continued flexion of the hips and continued ankle dorsiflexion in this phase. One of the most important

characteristics of this phase is that it has the largest amount of ground reaction force among all four phases of STS. This is because during this phase, all the body weight is on the feet. Looking at the pattern of Ground Reaction Force (GRF), we see that there is a basic need to produce ground force greater than body weight in order to accelerate the body in the upward direction [30].

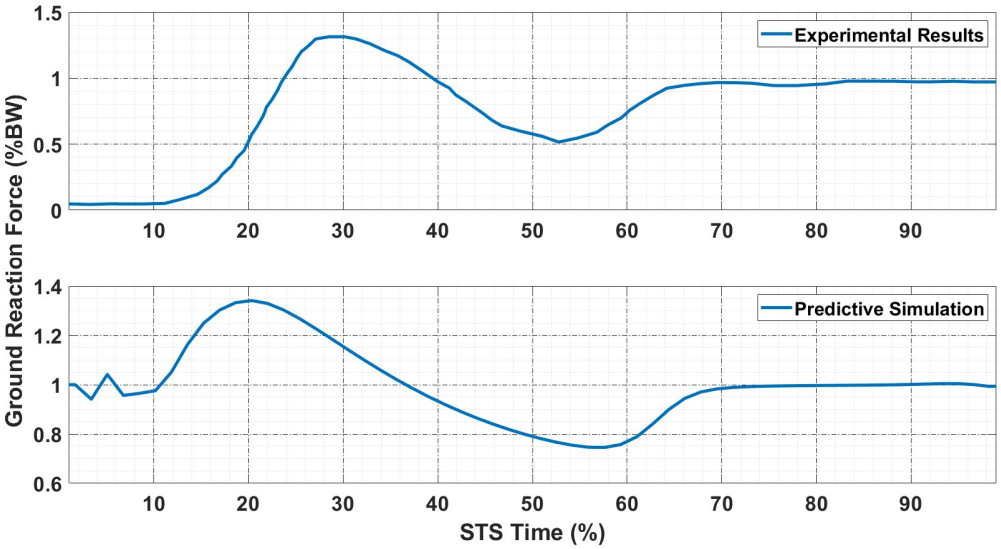


Figure 3. The profile of GRF directed forward under the feet from simulation and experimental results [30].

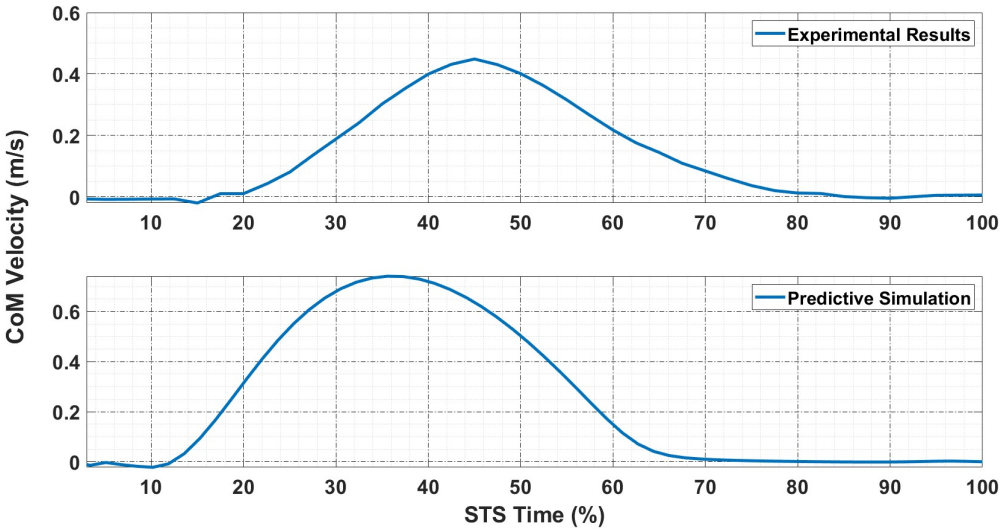


Figure 4. The velocity of COM of the model and the experimental results [29].

The third phase starts at maximum ankle dorsiflexion and ends at hip extension. It includes a sequence of lower limb extensions, knee extension, hip extension, and ankle extension. When a person stands up to a standing position from the point of maximum ankle dorsiflexion, the foot does not change position, but the tibia will move backward on the ankle. Therefore, the angle between tibia and the foot will be around 60° in this phase, whereas in the standing position it will be around 90°. In the previous phase, muscles are activated to flex the knee, whereas in this phase, the muscles are activated to extend the knee.

The GRF will start to decrease from its maximum value, indicating that the thigh is leaving the seat [30]. Again, the ground reaction force will start to increase once the body is in the upward standing position [31]. This phase is terminated once the hip reaches its maximum extension. The last phase is mainly about stabilizing the body and preventing

it from falling down, since the body is already in a standing position. In this phase, the velocity of COM will approach zero, indicating the termination of STS movement.

3.1. STS Speed

The effect of STS speed on joints' kinetic and kinematics was investigated using the three-links model by changing the time required to stand up from sitting position. In order to stand up from the sitting position, the model flexes the torso forward with the presence of the hip flexion. The results show that as the speed increases (time to stand up is reduced), the torso remains flexed for a longer time interval as a percentage of total STS duration, as seen in Figure 5. Additionally, at very short time of STS, the model stands up with a flexed torso. This means that the duration of the stabilization phase reduces as the speed increases. In addition to the increment in the flexion duration of the torso, the torso angular velocity tends to increase as the speed increases, as shown in Figure 6.

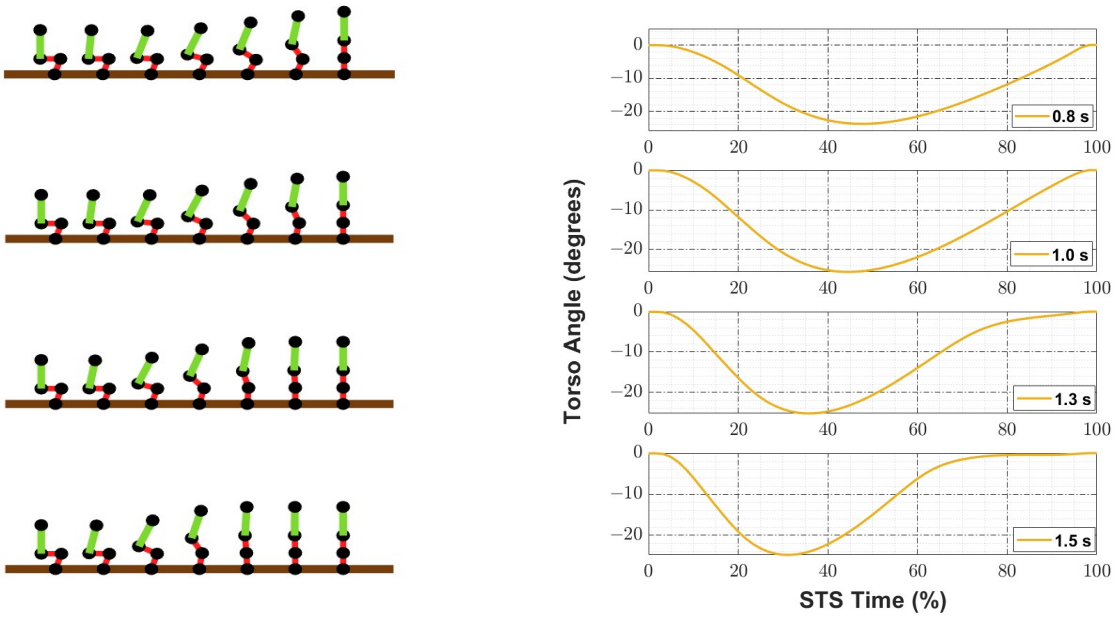


Figure 5. (**a**) The model performing the sit-to-stand task within different timeframes; (**b**) Torso angle during standing from sitting position within different timeframes.

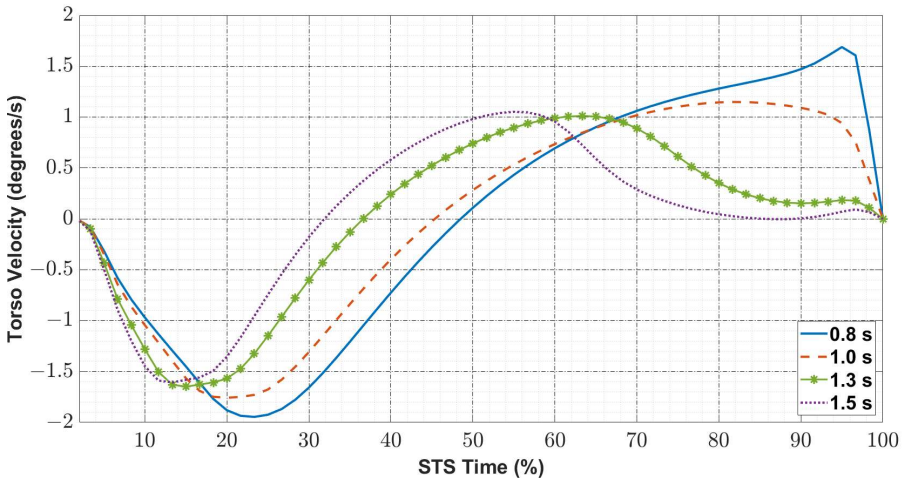


Figure 6. Torso angular velocity at different STS speeds.

An initial flexion angular velocity (negative) is observed at the hip joint as the torso is leaning forwards, followed by a positive angular velocity indicating the extension of the hip joint, which is continuous until the standing position is attained, as is clear from Figure 7. On the other hand, the velocity of the knee joint shows a smooth increase and decrease in the negative direction (extension velocity), demonstrating the control of the movement towards the full extension position, as shown in Figure 7. The peak of the angular velocity increases as the speed of rising increases, indicating the presence of exaggerated knee joint loading and causing an increment in the knee joint torque, as portrayed in Figure 8.

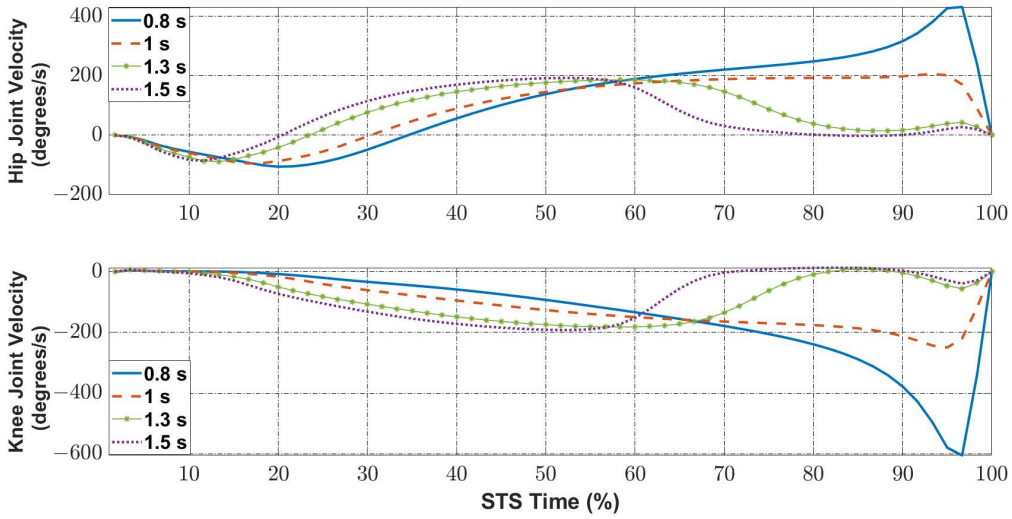


Figure 7. Hip joint velocity and knee joint velocity at different STS speeds.

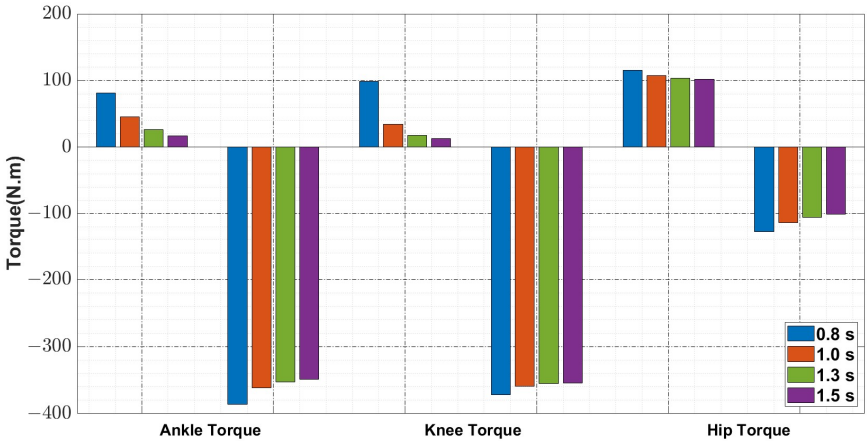


Figure 8. Ankle, knee, and hip torques at different STS speeds.

A sufficient torque needs to be generated at the joints to overcome the challenges that will need to be faced to accomplish this task successfully, including moving the body's center of mass forward and raising it vertically to the standing position.

The results have shown that the increment in the speed of STS increases the ankle dorsiflexion, knee extension, and hip flexion joint torques, and among the models' joints, the results of the optimization demonstrated that the knee is the most affected joint by increasing speed, as displayed in Figure 8.

3.2. Reduction in Joint Strength

To investigate the effect of reduced knee strength on STS motion, the model is used to optimize the STS motion with minimum joint torques and especially the knee joint torque. This can be accomplished by reformulating the cost function in Equation (7) to have a larger

coefficient for the knee joint torque. The optimizer was run with different coefficients for the knee joint torque (α_2 = 1, 3, 5, and 7). The results of the optimization showed that as the coefficient of knee joint torque increases, the model tends to flex the knee and the torso as well while standing up and start to extend them at the moment just before the standing position, which is as shown in Figure 9.

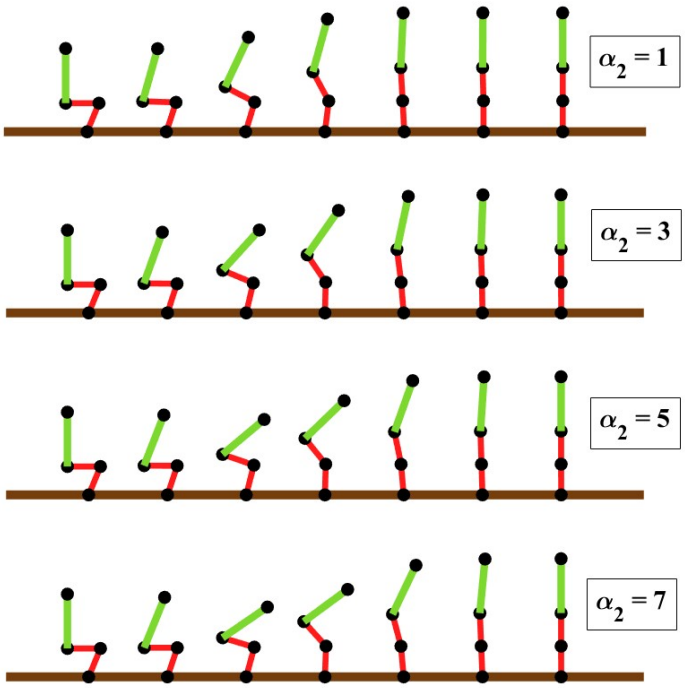


Figure 9. The model standing up with reduced knee joint strength corresponds to different coefficients of knee joint torque (α_2 = 1, α_2 = 3, α_2 = 5, and α_2 = 7).

Increasing the coefficient of knee joint torque to indicate the difficulties in rising due to the knee joint seems to increase the angular velocity of hip flexion and angular velocity of knee extension as seen in Figure 10. Moreover, an increment in the hip joint torque was observed in Figure 11 when increasing the coefficient of knee joint torque, indicating that the model depends on the hip joint to accommodate for the losing of some knee joint strength.

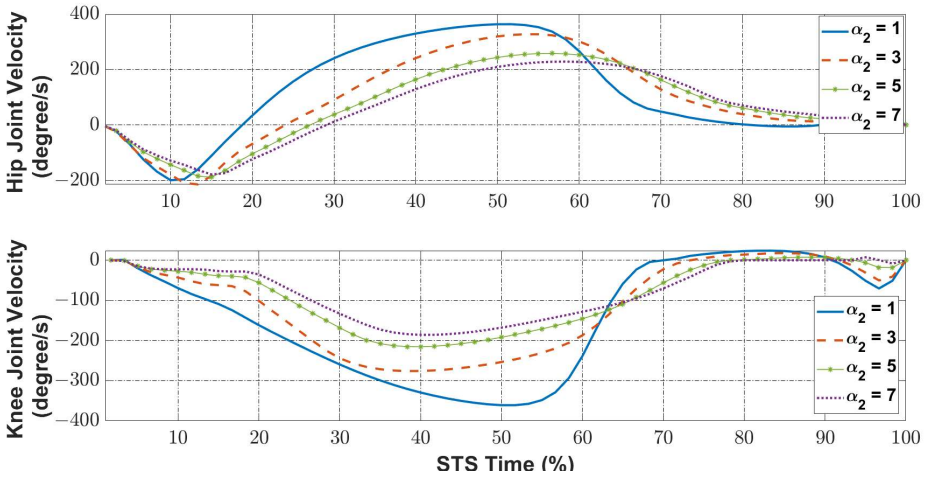


Figure 10. The angular velocity of the model with reduced knee joint strength corresponds to different coefficients of knee joint torque (α_2 = 1, α_2 = 3, α_2 = 5, and α_2 = 7).

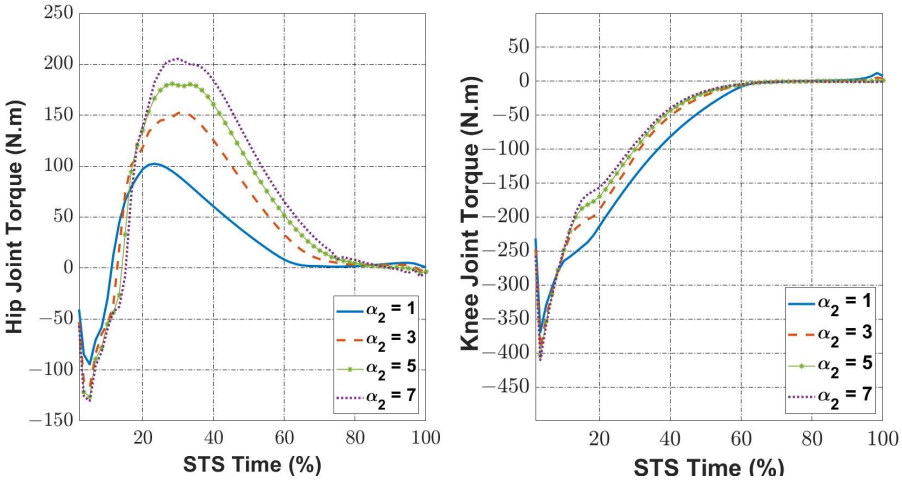


Figure 11. The Hip and knee joint torques of the model with reduced knee joint strength correspond to different coefficients of knee joint torque ($\alpha_2 = 1$, $\alpha_2 = 3$, $\alpha_2 = 5$, and $\alpha_2 = 7$).

Furthermore, the effect of reduced knee strength was studied at two speeds, fast and slow, corresponding to STS duration of 1.5 s and 0.8 s, respectively. The results of different STS speeds showed a similar pattern of joint motion, as shown in Figure 12. The model first flexed the hip while still at the sitting position with the knee initially flexed at 90°, and then performed a series of extension movements by extending the hip and knee (after a short delay) joints while plantar flexing the ankle during the remaining time of the standing. Immoderate hip flexion is resisted by the contraction of muscles, which at the same time motivates the knee flexion just prior standing up. Knee flexion is also controlled by the contraction of muscles to avoid excessive knee flexion. Figure 12 shows that the joint angle profiles for the case of larger knee torque coefficients were identical to the normal case at a slow speed; however, the range of joint motion with reduced knee strength was slightly decreased at a fast speed. On the other hand, for the same case (normal knee strength or reduced knee strength), increasing the speed resulted in increased joint range of motion.

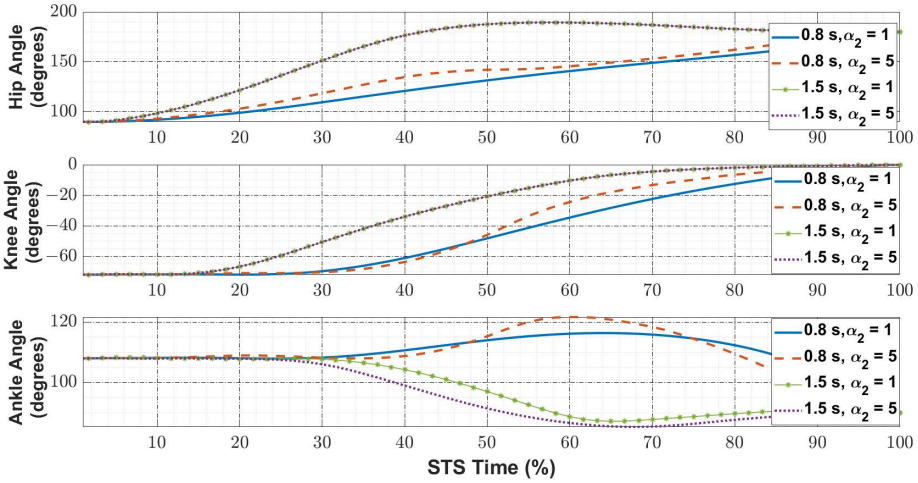


Figure 12. Hip angle, Knee angle, and Ankle angle at different STS speeds with normal and reduced knee joint strength ($\alpha_2 = 1$ and $\alpha_2 = 5$, respectively).

With normal knee strength, and as a consequence of a more upright torso during standing up, as stated in the previous section, the body's center of mass exhibited a more posterior location (behind the foot) in the cases of a fast speed that corresponds to a standing duration of 0.8 s and 1.0 s. However, with reduced knee strength, the increment in the speed increases the horizontal position of the center of mass, as seen in Figure 13. On the

other hand, with normal knee strength and reduced knee strength, the vertical position of the body's center of mass starts to increase earlier for the cases of slow motion, indicating that the torso is remaining flexed while standing up for the cases of fast motion. However, the impact of speed on the vertical position of center of mass is clearer for the case of reduced knee strength than normal knee strength.

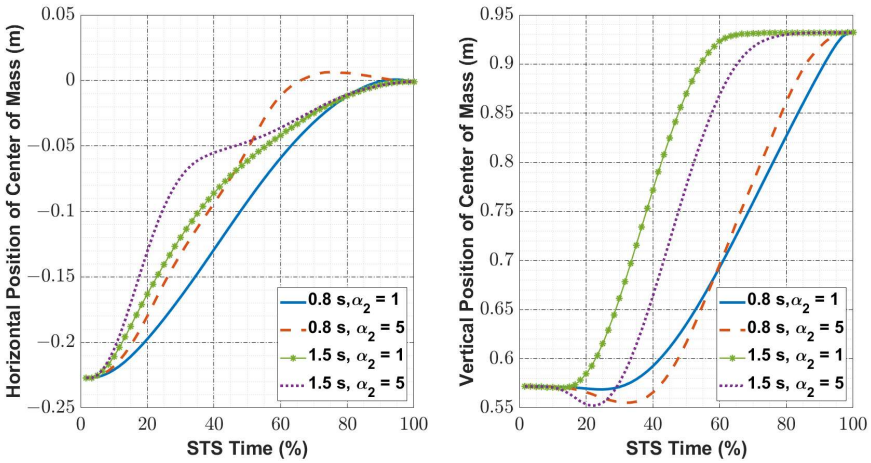


Figure 13. Horizontal and vertical positions of the center of mass at different STS speeds with normal and reduced knee joint strength (α_2 = 1 and α_2 = 5, respectively).

Figure 14 shows that the increment and decrement in the angular velocity of the hip and knee joints tends to be rough at a fast STS motion for α_2 = 5 with a significant increment in the peak value of knee angular velocity compared to the hip angular velocity.

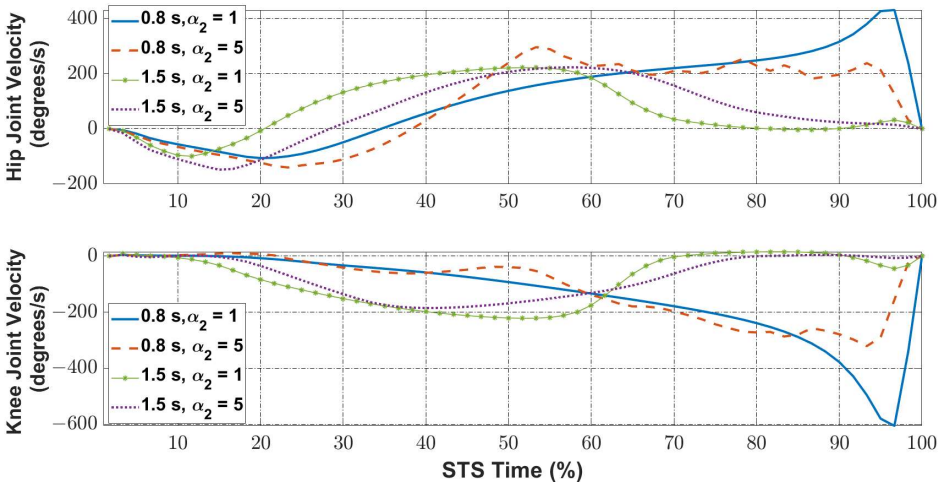


Figure 14. Hip joint velocity and knee joint velocity at different STS speeds with normal and reduced knee joint strength (α_2 = 1 and α_2 = 5, respectively).

3.3. Seat Height

The results of the optimization of four seat heights (30 cm, 33 cm, 37 cm, and 44 cm) showed almost a similar time taken by the model to stand from the sitting position, although the time required to attain the full standing position was longer for the lowest seat height. Moreover, the torso angle showed noticeable differences in the forward movement by showing an increment in the maximum torso angle, as seen in Figure 15, as the seat height decreases with larger angular displacements of the joints due to the larger space needing to be covered.

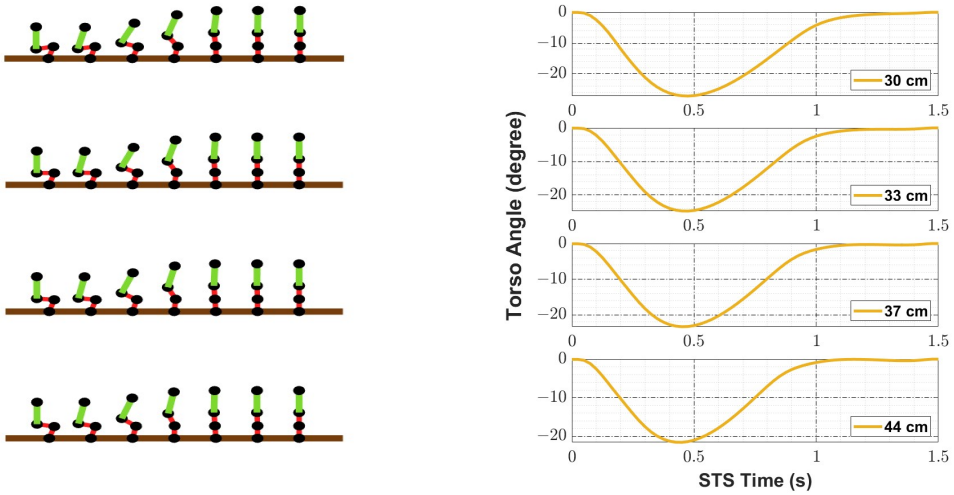


Figure 15. (**a**) Model standing up from different seat heights; (**b**) Torso angle of the model standing up from four seat heights (30 cm, 33 cm, 37 cm, and 44 cm).

The results apparently showed that as the seat height decreases, the hip and knee extension velocity increases, as seen in Figure 16, resulting in more foot repositioning, which led to an increase in the ground reaction force, as shown in Figure 17.

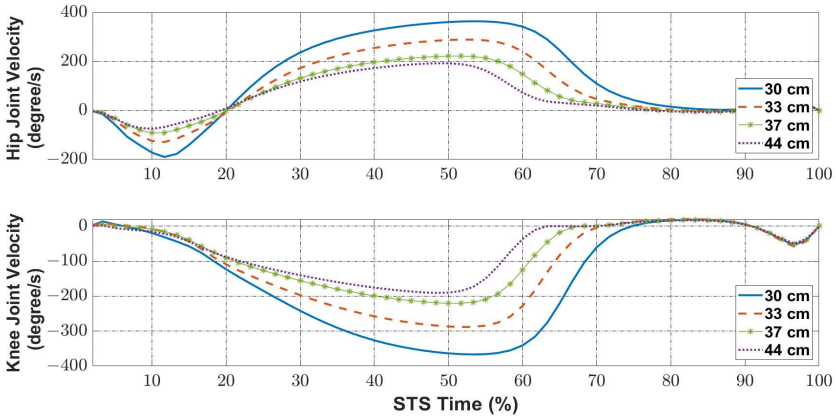


Figure 16. Hip and knee joint velocities of the model standing up from four seat heights (30 cm, 33 cm, 37 cm, and 44 cm).

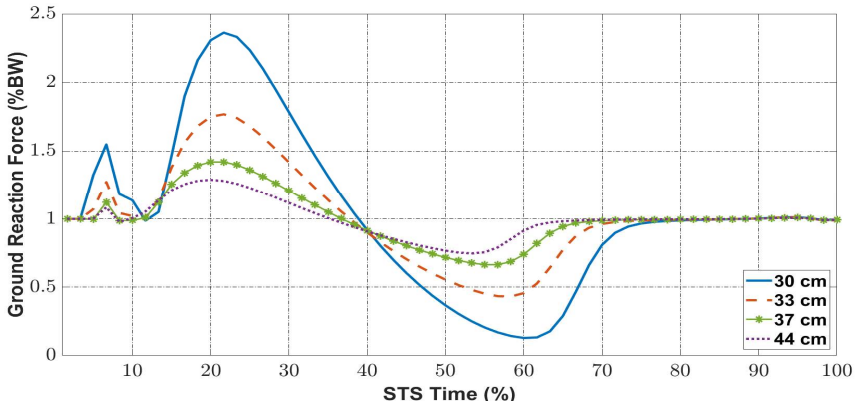


Figure 17. Ground Reaction Force of the model (as a percentage of body weight) standing up from four seat heights (30 cm, 33 cm, 37 cm, and 44 cm).

We have found that lowering the seat height increases the hip torque before and after the seat off, as well; however, reducing the height decreases the knee torque before seat off while increases it after seat off, as clear from Figure 18.

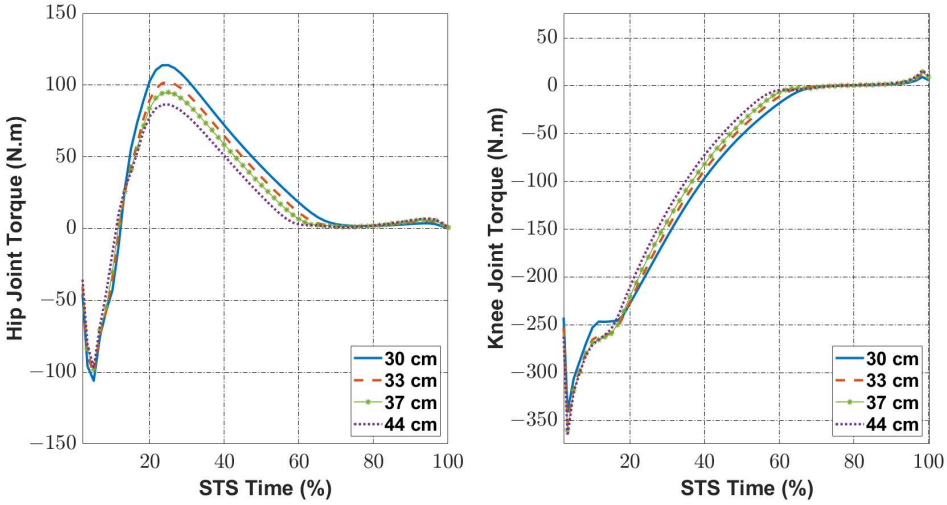


Figure 18. Hip joint and knee joint torque of the model standing up from four seat heights (30 cm, 33 cm, 37 cm, and 44 cm).

4. Discussion

We have found that increasing STS speed resulted in a shorter duration of STS phases, which agrees with reported experimental studies in the literature [32,33] and a more upright position of the torso at lift-off. Furthermore, in order to speed up the motion of STS by reducing the duration of phases, the joint torque was significantly affected, which agrees with reported experimental studies in the literature [7,13,34,35]. It is also found that increasing the speed of STS motion increased the hip flexion torque, knee extension torque, and ankle dorsiflexion torque for the model with both normal knee strength and reduced knee strength, and this validates the results of other experimental studies on healthy people and people with weakened knees [7,13,34,35]. However, between the model joints, the knee joint was the most affected joint, and it was clear from the significant increment in the knee extension moment and knee extension velocity [8,35]. This impact may be due to the load of body weight on the knee at the moment of standing up, since the model was standing with a flexed torso.

Therefore, due to the great increment in the knee joint torque, more attention was paid to the knee joint by increasing the coefficient of knee joint torque in the cost function to represent individuals with weakened or impaired knee joints, such as patients with some knee osteoarthritis or elderly people, and investigated the effect of this on STS motion. Furthermore, it was observed that as the strength of the knee joint was reduced (increasing the coefficient of knee joint torque), the angular velocities of hip and knee joints slightly increased; however, the increment in the hip joint torque was very significant. This indicated that the hip joint was trying to compensate for the reduction in the available knee joint torque. To avoid the load on the knee joint, a person can stand up slowly, especially when there are abnormalities in the knee joint; however, fast STS motion is required not only as a daily life activity, but also to do some clinical settings and tests like fast STS tests, in which patients are asked to stand up as quickly as possible. Regarding the kinetic parameters of lower limb joints and how they are affected by speed, the results of fast STS motion for the model with normal and reduced knee strength was characterized by increased knee and hip peak velocities, similar results being reported in experimental studies in the literature [7,8] and they tended to be unsmooth at fast speed as we increased the coefficient of knee joint torque. We have found that as the speed of motion was increased, the horizontal position of center of mass also increased, which can be related to the upright position of the

torso while standing up, and the results of this simulation are in agreement with reported experimental studies reported in the literature [35,36]. However, the pattern of lower limb joints, including the hip, was similar when performing STS motion at fast and slow speeds for both normal knee strength and reduced knee strength [36].

Conversely, we have investigated the effects of seat height on the kinetic and kinematic parameters of the model during STS motion, as it has been considered as the most influential factor related to the chair properties [16,37,38]. The results indicated that reducing the seat height increases the angular velocity of the hip and knee joints required to stand up, which was a consequence of the increment in the torso angular velocity required to move the torso further forward from a lower seat height before seat off [16,37,38]. The higher angular velocity resulted in a higher torque at the hip joint, which transferred to the lower limb joints after leaving the seat. It is also noticed that the model exhibited an increment in the torso movement which was demonstrated by Weiner et al. as a result of increasing the demand to move the center of mass closer to the knees and reduce the required effort [39]. The higher torque at the hip joint was used by the model to assist in the remaining phases of STS, which was also due to the high forward velocity of the torso at seat off [39]. The increment in the joints' angular displacement exhibited by the model as the seat height is decreased is also confirmed by other studies [11,40], and the reason behind that was demonstrated by Yamada and Demura as reported in [17] that standing up from a lower seat height is more difficult due to the increment in the distance that must be covered by the person in order to stand up. The increase in the distance covered will also lead to an increment in the muscle activity of the lower limbs, which is represented by the increment of the model's joint torques in this study [11]. It has been known that the increment in the torso's forward movement increases the chance of falling down due to the huge torso mass compared to lower limbs; therefore, more feet repositioning was observed by the model when lowering the seat height as a stabilizing strategy [37,38], which resulted in an increment in the peak of the ground reaction force.

5. Conclusions

In this study, we have used a mathematical model to investigate its ability to predict STS body adaptations by formulating an optimization problem that minimizes joints' torques. The model was able to predict basic features of STS motion by following the constraints of the optimization problem. We have found that STS motion may be influenced by different factors such as motion speed, reduced joint strength, and seat height. We have first investigated the effect of motion speed by changing the total time required to stand up from the sitting position while equally optimizing the joint torques. Then, we reduced the knee joint strength, since it was the most affected joint, by increasing the coefficient of joint torque in the cost function for the purpose of optimizing it more than the other joints torques. Finally, we studied the effect of seat height on the STS motion by changing the femur link to get different seat heights, and again equally optimized the joints torque.

The results of this study for the three cases agreed with published experimental results, indicating that the model was able to predict the STS body adaptation. Increasing STS motion speed, reducing knee strength, and reducing seat height was found to increase joints torque and joints angular velocity, whereas reducing the knee strength was found to decrease the range of joints motion. On the other hand, we have found that reducing knee strength and reducing seat height led to increased torso flexion, while increasing STS motion speed led to standing up with an upright torso position. Moreover, the model expressed higher ground reaction force as the height of the seat was reduced and more posterior center of mass position as the knee strength was reduced.

Since STS motion is used for clinical investigation as well as daily activity as human beings, it is very important to pay attention to the factors that may impact this motion. Therefore, the model involved in this study can help in understanding these factors and determining the ability of the person to complete this motion and the challenges that may be faced.

Author Contributions: Conceptualization, S.G., A.A.-Y. and R.Z.; methodology, S.G.; software, S.G.; validation, S.G.; formal analysis, S.G., A.A.-Y. and R.Z.; investigation, S.G., A.A.-Y. and R.Z.; resources, S.G.; data curation, S.G.; writing—original draft preparation, S.G.; writing—review and editing, S.G., A.A.-Y., R.Z., H.O. and I.B.; visualization, S.G., A.A.-Y. and R.Z.; supervision, A.A.-Y. and R.Z.; project administration, A.A.-Y. All authors have read and agreed to the published version of the manuscript.

Funding: This research was funded by the former Research Council, grant number RC/ENG/MIED/15/2.

Data Availability Statement: Not applicable.

Acknowledgments: The authors would like to thank Sultan Qaboos University (SQU) and the former Research Council for supporting this research.

Conflicts of Interest: The authors declare no conflict of interest.

Appendix A

The model under study consists of three segments: the torso, the femur, and the tibia. This model is simplified as we study human motion in the sagittal plane in which we can assume that the two legs move in an asymmetric manner, so we can include one leg only. The system dynamics are derived using direct discretization of the Lagrange-d'Alembert Principle (discrete mechanics). First, we define the positions of center of mass of each link in the x and y coordinates:

$$x_{c1} = -(l_1 - d_1)sin\theta_1 \tag{A1}$$

$$y_{c1} = (l_1 - d_1)cos\theta_1 \tag{A2}$$

$$x_{c2} = -l_1 sin\theta_1 - (l_2 - d_2)sin\theta_2 \tag{A3}$$

$$y_{c2} = l_1 cos\theta_1 + (l_2 - d_2)cos\theta_2 \tag{A4}$$

$$x_{c3} = -l_1 sin\theta_1 - l_2 sin\theta_2 - (l_3 - d_3)sin\theta_3 \tag{A5}$$

$$y_{c3} = l_1 cos\theta_1 + l_2 cos\theta_2 + (l_3 - d_3)cos\theta_3 \tag{A6}$$

The velocities of center of mass of each link in the x and y coordinates are:

$$\dot{x}_{c1} = -(l_1 - d_1)\dot{\theta}_1 cos\theta_1 \tag{A7}$$

$$\dot{y}_{c1} = -(l_1 - d_1)\dot{\theta}_1 sin\theta_1 \tag{A8}$$

$$\dot{x}_{c2} = -l_1\dot{\theta}_1 cos\theta_1 - (l_2 - d_2)\dot{\theta}_2 cos\theta_2 \tag{A9}$$

$$\dot{y}_{c2} = -l_1\dot{\theta}_1 sin\theta_1 - (l_2 - d_2)\dot{\theta}_2 sin\theta_2 \tag{A10}$$

$$\dot{x}_{c3} = -l_1\dot{\theta}_1 cos\theta_1 - l_2\dot{\theta}_2 cos\theta_2 - d_3\dot{\theta}_3 cos\theta_3 \tag{A11}$$

$$\dot{y}_{c3} = -l_1\dot{\theta}_1 sin\theta_1 - l_2\dot{\theta}_2 sin\theta_2 - d_3\dot{\theta}_3 sin\theta_3 \tag{A12}$$

The kinetic energy of each link:

$$KE_1 = \frac{1}{2}m_1 v_{c1}^2 = \frac{1}{2}m_1(l_1 - d_1)^2\dot{\theta}_1^2 + \frac{1}{2}I_1\dot{\theta}_1^2 \tag{A13}$$

$$KE_2 = \frac{1}{2}m_2 v_{c2}^2 = \frac{1}{2}m_2 l_1^2\dot{\theta}_1^2 + \frac{1}{2}m_2(l_2 - d_2)^2\dot{\theta}_2^2 + \frac{1}{2}I_2\dot{\theta}_2^2 + m_2 l_1(l_2 - d_2)\dot{\theta}_1\dot{\theta}_2 cos(\theta_1 - \theta_2) \tag{A14}$$

$$\begin{aligned} KE_3 = \tfrac{1}{2}m_3v_{c3}^2 = \quad & \tfrac{1}{2}m_3l_1^2\dot{\theta}_1^2 + \tfrac{1}{2}m_3l_2^2\dot{\theta}_2^2 + \tfrac{1}{2}m_3(l_3-d_3)^2\dot{\theta}_3^2 + \tfrac{1}{2}I_3\dot{\theta}_3^2 \\ & + m_3l_1l_2\dot{\theta}_1\dot{\theta}_2cos(\theta_1-\theta_2) + m_3l_1(l_3-d_3)\dot{\theta}_1\dot{\theta}_3cos(\theta_1-\theta_3) \\ & + m_3l_2(l_3-d_3)\dot{\theta}_2\dot{\theta}_3cos(\theta_2-\theta_3) \end{aligned} \tag{A15}$$

The potential energy of each link:

$$PE_1 = m_1gy_1 = m_1g(l_1-d_1)cos\theta_1 \tag{A16}$$

$$PE_2 = m_2gy_2 = m_2gl_1cos\theta_1 + m_2g(l_2-d_2)cos\theta_2 \tag{A17}$$

$$PE_3 = m_3gy_3 = m_3gl_1cos\theta_1 + m_3gl_2cos\theta_2 + m_3g(l_3-d_3)cos\theta_3 \tag{A18}$$

Now we derive the Lagrange equation of the model:

$$\mathcal{L} = total\ kinetic\ energy - total\ potential\ energy = KE - PE \tag{A19}$$

$$\begin{aligned} \mathcal{L} = \tfrac{1}{2}\Big(m_1(l_1-d_1)^2 \quad & + m_2l_1^2 + m_3l_1^2\Big)\dot{\theta}_1^2 + \tfrac{1}{2}\Big(m_2(l_2-d_2)^2 + m_3l_2^2\Big)\dot{\theta}_2^2 + \tfrac{1}{2}m_3d_3^2\dot{\theta}_3^2 \\ & - (m_2l_1(l_2-d_2) + m_3l_1l_2)\dot{\theta}_1\dot{\theta}_2cos(\theta_1+\theta_2) \\ & + m_3l_1d_3\dot{\theta}_1\dot{\theta}_3cos(\theta_1-\theta_3) - m_3l_2d_3\dot{\theta}_2\dot{\theta}_3cos(\theta_2+\theta_3) \\ & - g(m_1(l_1-d_1) + m_2l_1 + m_3l_1)cos\theta_1 \\ & - g(m_2(l_2-d_2) + m_3l_2)cos\theta_2 - m_3gd_3cos\theta_3 \end{aligned} \tag{A20}$$

Now we convert the continuous Lagrange equation into a discrete Lagrange equation using the mid-point rule as follows:

$$\mathcal{L}(q,\dot{q}) \to h\mathcal{L}_d\left(\frac{q_{k+1}+q_k}{2}, \frac{q_{k+1}-q_k}{h}\right) \tag{A21}$$

$$\begin{aligned} L_d = \tfrac{1}{2h}a_1\Delta\theta_{1k}{}^2 + \quad & \tfrac{1}{2h}a_2\Delta\theta_{2k}{}^2 + \tfrac{1}{2h}a_3\Delta\theta_{3k}{}^2 + \tfrac{1}{h}b_1\Delta\theta_{1k}\Delta\theta_{2k}cos\Big(\tfrac{\sum\theta_{1k}}{2} - \tfrac{\sum\theta_{2k}}{2}\Big) \\ & + \tfrac{1}{h}b_2\Delta\theta_{1k}\Delta\theta_{3k}cos\Big(\tfrac{\sum\theta_{1k}}{2} - \tfrac{\sum\theta_{3k}}{2}\Big) \\ & + \tfrac{1}{h}b_3\Delta\theta_{2k}\Delta\theta_{3k}cos\Big(\tfrac{\sum\theta_{2k}}{2} - \tfrac{\sum\theta_{3k}}{2}\Big) - ghc_1cos\Big(\tfrac{\sum\theta_{1k}}{2}\Big) \\ & - ghc_2cos\Big(\tfrac{\sum\theta_{2k}}{2}\Big) - ghc_3cos\Big(\tfrac{\sum\theta_{3k}}{2}\Big) \end{aligned} \tag{A22}$$

where:

$$a_1 = I_1 + m_1(l_1-d_1)^2 + m_2l_1^2 + m_3l_1^2 \tag{A23}$$

$$a_2 = I_2 + m_2(l_2-d_2)^2 + m_3l_2^2 \tag{A24}$$

$$a_3 = I_3 + m_3(l_3-d_3)^2 \tag{A25}$$

$$b_1 = m_2l_1(l_2-d_2) + m_3l_1l_2 \tag{A26}$$

$$b_2 = m_3l_1(l_3-d_3) \tag{A27}$$

$$b_3 = m_3l_2(l_3-d_3) \tag{A28}$$

$$c_1 = m_1(l_1-d_1) + m_2l_1 + m_3l_1 \tag{A29}$$

$$c_2 = m_2(l_2 - d_2) + m_3 l_2 \tag{A30}$$

Now find $D_1L_d(\theta_{1k}, \theta_{1k+1}, \theta_{2k}, \theta_{2k+1}, \theta_{3k}, \theta_{3k+1})$ and $D_2L_d(\theta_{1k}, \theta_{1k+1}, \theta_{2k}, \theta_{2k+1}, \theta_{3k}, \theta_{3k+1})$.

$D_1L_d(\theta_{1k}, \theta_{1k+1}, \theta_{2k}, \theta_{2k+1}, \theta_{3k}, \theta_{3k+1})$: The first derivative of the discrete Lagrange with respect to the current coordinates (i.e., θ_{1k}, θ_{2k}, and θ_{3k})

$$\begin{aligned} D_1\mathcal{L}_d = \tfrac{\partial \mathcal{L}_d}{\partial \theta_{1k}} \quad & (\theta_{1k}, \theta_{1k+1}, \theta_{2k}, \theta_{2k+1}, \theta_{3k}, \theta_{3k+1}) \\ & = -\tfrac{1}{h}a_1\Delta\theta_{1k} - \tfrac{1}{h}b_1\Delta\theta_{2k}cos\Big(\tfrac{\sum\theta_{1k}}{2} - \tfrac{\sum\theta_{2k}}{2}\Big) \\ & -\tfrac{1}{2h}b_1\Delta\theta_{1k}\Delta\theta_{2k}sin\Big(\tfrac{\sum\theta_{1k}}{2} - \tfrac{\sum\theta_{2k}}{2}\Big) - \tfrac{1}{h}b_2\Delta\theta_{3k}cos\Big(\tfrac{\sum\theta_{1k}}{2} - \tfrac{\sum\theta_{3k}}{2}\Big) \\ & -\tfrac{1}{2h}b_2\Delta\theta_{1k}\Delta\theta_{3k}sin\Big(\tfrac{\sum\theta_{1k}}{2} - \tfrac{\sum\theta_{3k}}{2}\Big) + \tfrac{ghc_1}{2}sin\Big(\tfrac{\sum\theta_{1k}}{2}\Big) \end{aligned} \tag{A31}$$

$$\begin{aligned} D_1\mathcal{L}_d = \tfrac{\partial \mathcal{L}_d}{\partial \theta_{2k}} \quad & (\theta_{1k}, \theta_{1k+1}, \theta_{2k}, \theta_{2k+1}, \theta_{3k}, \theta_{3k+1}) \\ & = -\tfrac{1}{h}a_2\Delta\theta_{2k} - \tfrac{1}{h}b_1\Delta\theta_{1k}cos\Big(\tfrac{\sum\theta_{1k}}{2} - \tfrac{\sum\theta_{2k}}{2}\Big) \\ & +\tfrac{1}{2h}b_1\Delta\theta_{1k}\Delta\theta_{2k}sin\Big(\tfrac{\sum\theta_{1k}}{2} - \tfrac{\sum\theta_{2k}}{2}\Big) - \tfrac{1}{h}b_3\Delta\theta_{3k}cos\Big(\tfrac{\sum\theta_{2k}}{2} - \tfrac{\sum\theta_{3k}}{2}\Big) \\ & -\tfrac{1}{2h}b_3\Delta\theta_{2k}\Delta\theta_{3k}sin\Big(\tfrac{\sum\theta_{2k}}{2} - \tfrac{\sum\theta_{3k}}{2}\Big)\tfrac{ghc_2}{2}sin\Big(\tfrac{\sum\theta_{2k}}{2}\Big) \end{aligned} \tag{A32}$$

$$\begin{aligned} D_1\mathcal{L}_d = \tfrac{\partial \mathcal{L}_d}{\partial \theta_{3k}} \quad & (\theta_{1k}, \theta_{1k+1}, \theta_{2k}, \theta_{2k+1}, \theta_{3k}, \theta_{3k+1}) \\ & = -\tfrac{1}{h}a_3\Delta\theta_{3k} - \tfrac{1}{h}b_2\Delta\theta_{1k}cos\Big(\tfrac{\sum\theta_{1k}}{2} - \tfrac{\sum\theta_{3k}}{2}\Big) \\ & +\tfrac{1}{2h}b_2\Delta\theta_{1k}\Delta\theta_{3k}sin\Big(\tfrac{\sum\theta_{1k}}{2} - \tfrac{\sum\theta_{3k}}{2}\Big) - \tfrac{1}{h}b_3\Delta\theta_{2k}cos\Big(\tfrac{\sum\theta_{2k}}{2} - \tfrac{\sum\theta_{3k}}{2}\Big) \\ & +\tfrac{1}{2h}b_3\Delta\theta_{2k}\Delta\theta_{3k}sin\Big(\tfrac{\sum\theta_{2k}}{2} - \tfrac{\sum\theta_{3k}}{2}\Big) + \tfrac{ghc_3}{2}sin\Big(\tfrac{\sum\theta_{3k}}{2}\Big) \end{aligned} \tag{A33}$$

$D_2L_d(\theta_{1k}, \theta_{1k+1}, \theta_{2k}, \theta_{2k+1}, \theta_{3k}, \theta_{3k+1})$: The first derivative of the discrete Lagrange with respect to the current coordinates (i.e.,θ_{1k+1}, θ_{2k+1}, and θ_{3k+1})

$$\begin{aligned} D_2\mathcal{L}_d = \tfrac{\partial \mathcal{L}_d}{\partial \theta_{1k+1}} \quad & (\theta_{1k}, \theta_{1k+1}, \theta_{2k}, \theta_{2k+1}, \theta_{3k}, \theta_{3k+1}) \\ & = \tfrac{1}{h}a_1\Delta\theta_{1k} + \tfrac{1}{h}b_1\Delta\theta_{2k}cos\Big(\tfrac{\sum\theta_{1k}}{2} - \tfrac{\sum\theta_{2k}}{2}\Big) \\ & -\tfrac{1}{2h}b_1\Delta\theta_{1k}\Delta\theta_{2k}sin\Big(\tfrac{\sum\theta_{1k}}{2} - \tfrac{\sum\theta_{2k}}{2}\Big) + \tfrac{1}{h}b_2\Delta\theta_{3k}cos\Big(\tfrac{\sum\theta_{1k}}{2} - \tfrac{\sum\theta_{3k}}{2}\Big) \\ & -\tfrac{1}{2h}b_2\Delta\theta_{1k}\Delta\theta_{3k}sin\Big(\tfrac{\sum\theta_{1k}}{2} - \tfrac{\sum\theta_{3k}}{2}\Big) + ghc_1sin\Big(\tfrac{\sum\theta_{1k}}{2}\Big) \end{aligned} \tag{A34}$$

$$\begin{aligned} D_2\mathcal{L}_d = \tfrac{\partial \mathcal{L}_d}{\partial \theta_{2k+1}} \quad & (\theta_{1k}, \theta_{1k+1}, \theta_{2k}, \theta_{2k+1}, \theta_{3k}, \theta_{3k+1}) \\ & = \tfrac{1}{h}a_2\Delta\theta_{2k} + \tfrac{1}{h}b_1\Delta\theta_{1k}cos\Big(\tfrac{\sum\theta_{1k}}{2} - \tfrac{\sum\theta_{2k}}{2}\Big) \\ & +\tfrac{1}{2h}b_1\Delta\theta_{1k}\Delta\theta_{2k}sin\Big(\tfrac{\sum\theta_{1k}}{2} - \tfrac{\sum\theta_{2k}}{2}\Big) + \tfrac{1}{h}b_3\Delta\theta_{3k}cos\Big(\tfrac{\sum\theta_{2k}}{2} - \tfrac{\sum\theta_{3k}}{2}\Big) \\ & -\tfrac{1}{2h}b_3\Delta\theta_{2k}\Delta\theta_{3k}sin\Big(\tfrac{\sum\theta_{2k}}{2} - \tfrac{\sum\theta_{3k}}{2}\Big) + ghc_2sin\Big(\tfrac{\sum\theta_{2k}}{2}\Big) \end{aligned} \tag{A35}$$

$$\begin{aligned} D_2\mathcal{L}_d = \tfrac{\partial \mathcal{L}_d}{\partial \theta_{3k+1}} \quad & (\theta_{1k}, \theta_{1k+1}, \theta_{2k}, \theta_{2k+1}, \theta_{3k}, \theta_{3k+1}) \\ & = \tfrac{1}{h}a_3\Delta\theta_{3k} + \tfrac{1}{h}b_2\Delta\theta_{1k}cos\Big(\tfrac{\sum\theta_{1k}}{2} - \tfrac{\sum\theta_{3k}}{2}\Big) \\ & +\tfrac{1}{2h}b_2\Delta\theta_{1k}\Delta\theta_{3k}sin\Big(\tfrac{\sum\theta_{2k}}{2} - \tfrac{\sum\theta_{3k}}{2}\Big) + \tfrac{1}{h}b_3\Delta\theta_{2k}cos\Big(\tfrac{\sum\theta_{1k}}{2} - \tfrac{\sum\theta_{3k}}{2}\Big) \\ & +\tfrac{1}{2h}b_3\Delta\theta_{2k}\Delta\theta_{3k}sin\Big(\tfrac{\sum\theta_{2k}}{2} - \tfrac{\sum\theta_{3k}}{2}\Big) + ghc_3sin\Big(\tfrac{\sum\theta_{3k}}{2}\Big) \end{aligned} \tag{A36}$$

After several investigations, we came out with the proper and most commonly used set of anthropometric information. Table A1 provides the weight of each segment as a percentage of the total body weight, the length of each segment as a percentage of total body height [25,26], the location of Center of Mass (COM) of each segment, measured as percentage of segment length [26], the segments' radius of gyration in the frontal plane (perpendicular to the sagittal plane) as a percentage of segment length [24], and it will be used to calculate the Moment of Inertia (MOI) for each segment. Based on this information, the required anthropometric data of the model is calculated for a male with 70 kg mass and 1.70 m height.

Table A1. Anthropometric percentages of different body segments required for the model.

Body Segment	Segment Mass as a PERCENTAGE of Body Mass	Segment Length as a Percentage of Total Body Height	Distance of Segment COM from Proximal End as a Percentage of Segment Length	Radius of Gyration of Body Segments in Frontal Plane as a Percentage of Segment Length
Head and Neck	8.2	10.75	56.7	31.5
Trunk	46.84	30.00	56.2	38.3
Upper arm	3.25	17.20	43.6	31.0
Forearm	1.8	15.70	43.0	28.4
Hand	0.65	5.75	46.8	23.3
Thigh	10.5	23.20	43.3	26.7
Calf	4.75	24.70	43.4	27.5

The moment of inertia for each segment is calculated using the anthropometric data associated with each segment. For instance, evaluation of MOI of the head and neck will be as follows:

- Mass of the head and neck segment is considered to be 8.2% of total body mass according to the data provided in Table A1, and hence, $m_{HN} = 5.78$ kg.
- According to Table A1, the length of the head and neck segment is 10.75% of the body height and is found to be $L_{HN} = 0.18$ m.
- Radius of gyration of the head and neck in the frontal axis is 31.5%, and hence, $k_{HN} = 0.058$ m.
- Now, the MOI of the head and neck can be determined using the following equation:

$$I_{HN} = m_{HN}k_{HN}^2 = 5.78 \times 0.058^2 = 0.0192 \text{ kg·m}^2 \tag{A37}$$

Using the same technique, the MOI of torso, hand segments, and leg segments are calculated, and the values are given in Table A2 with the other anthropometric measurements of each segment. The mass and moment of inertia of the head, the arms, and the torso (HAT) segment is simply found by summing up the individual mass of these segments; however, the center of mass is found using the parallel axis theorem [41]:

$$m_{HAT}d_{HAT} = m_{HN}d_{HN} + m_T d_T + 2 * m_{UA}d_{UA} + 2 * m_{FA}d_{FA} + 2 * m_H d_H \tag{A38}$$

The distance of the COM of the head and neck from the top of the head is d_{HN} and is calculated directly from Table A1. The distance of the COM of the torso from the top of the head is d_T, and it is equivalent to the total length of the head and neck segment and the distance from the neck to the COM of the torso. The same procedure is followed to calculate the distance from the top of the head to the COM of each segment of the arm.

$$\begin{aligned}(5.78 + 32.8 + 2 \times 2.275 \quad &+2 \times 1.309 + 2 \times 0.455)d_{HAT} \\ &= 5.78 \times 0.078 + 32.8 \times 0.4034 + 2 \times 2.275 \times 0.3075 + 2 \times 1.309 \times 0.585 \\ &+2 \times 0.455 \times 0.84\end{aligned} \tag{A39}$$

$$d_{HAT} = \frac{17.379}{46.66} = 0.3725 \text{ m} \tag{A40}$$

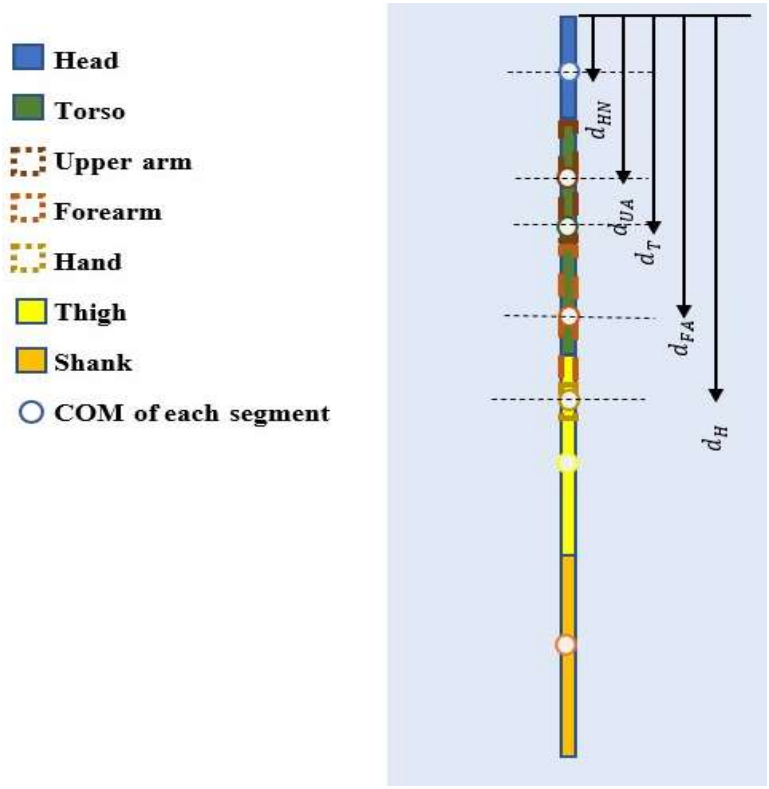


Figure A1. COM of body segments in the sagittal plane.

The MOI of upper body segments around the axis of rotation, which is the *y*-axis, can be approximated using the principle Parallel Axes Theorem. For applying the theorem, we need to determine the offset (r) for each segment, which is the shortest distance between the axis of rotation and the other axis passing through the COG of that segment. For example, the offset distance between the axis of rotation and the axis of the head and neck segment is defined as r_{HN}, and it can be found as the distance between the COG of the head and neck segment to the joint of the shoulder and the distance from the joint of the shoulder to the COG of the HAT segment.

$$r_{HN} = d_{HAT} - d_{HN} = 0.3725 - 0.078 = 0.2945 \text{ m} \tag{A41}$$

The MOI of the head and neck about the axis of rotation is found as shown below.

$$I_{HN}{}' = I_{HN} + m_{HN} r_{HN}^2 = 0.0192 + \left(5.78 \times 0.2945^2\right) = 0.5205 \text{ kg·m}^2 \tag{A42}$$

Using the same procedure, we found the offset distances and the moments of inertia about the axis of rotation for the other segments:

For the torso:

$$r_T = d_T - d_{HAT} = 0.4034 - 0.3725 = 0.0309 \text{ m} \tag{A43}$$

$$I_T{}' = I_T + m_T r_T^2 = 1.251 + \left(32.8 \times 0.0309^2\right) = 1.2823 \text{ kg·m}^2 \tag{A44}$$

For the upper arms:

$$r_{UA} = d_{HAT} - d_{UA} = 0.3725 - 0.3075 = 0.065 \text{ m} \tag{A45}$$

$$I_{UA}{}' = I_{UA} + m_{UA}r_{UA}^2 = 0.0187 + \left(2.275 \times 0.065^2\right) = 0.0283 \text{ kg·m}^2 \quad \text{(A46)}$$

For the forearms:

$$r_{FA} = d_{FA} - d_{HAT} = 0.585 - 0.3075 = 0.2775 \text{ m} \quad \text{(A47)}$$

$$I_{FA}{}' = I_{FA} + m_{FA}r_{FA}^2 = 0.00752 + \left(1.309 \times 0.2775^2\right) = 0.1083 \text{ kg·m}^2 \quad \text{(A48)}$$

For the hands:

$$r_H = d_H - d_{HAT} = 0.84 - 0.3075 = 0.5325 \text{ m} \quad \text{(A49)}$$

$$I_H{}' = I_H + m_H r_H^2 = 0.000236 + \left(0.455 \times 0.5325^2\right) = 0.1292 \text{ kg·m}^2 \quad \text{(A50)}$$

Then, the total MOI of the HAT segment about the axis of rotation is found by summing up the MOI of the individual segments about the same axis of rotation:

$$\begin{aligned} I_{HAT}{}' &= I_{HN}{}' + I_T{}' + I_{UA}{}' + I_{FA}{}' + I_H{}' \\ &= 0.5205 + 1.2823 + 0.0283 + 0.1083 + 0.1292 = 2.0686 \text{ kg·m}^2 \end{aligned} \quad \text{(A51)}$$

The table below shows the physical parameters for a male with 70 kg and 1.70 m required to build the model. Since the model does not include the head and the arms, the head and the three segments of the arms will be considered as one segment with the torso, represented as HAT (Head, Arms, and Torso).

Table A2. Model physical parameters based on a male with 70 kg mass and 1.70 m height.

Body Segment	Segment Mass (KG)	Segment Length (m)	Distance of Segment COM from Proximal (m)	Moment of Inertia
Head & Neck	0.18	5.782	0.10361925	0.019160814
Trunk	0.51	32.788	0.28662	1.250987086
Upper arm	0.29	2.275	0.1274864	0.018692162
Forearm	0.27	1.309	0.1155677	0.007520963
Hand	0.10	0.455	0.045747	0.000236024
Thigh	0.39	7.35	0.1707752	0.081504892
Calf	0.42	3.325	0.1822366	0.044335212
HAT	0.69	46.648	0.214937	2.0686

References

1. Dorn, T.W.; Wang, J.M.; Hicks, J.L.; Delp, S.L. Predictive simulation generates human adaptations during loaded and inclined walking. *PLoS ONE* **2015**, *10*, e0121407. [CrossRef] [PubMed]
2. Abdel-Malek, K.; Arora, J. *Human Motion Simulation: Predictive Dynamics*; Academic Press: Cambridge, MA, USA, 2013.
3. Geyer, H. Simple Models of Legged Locomotion Based on Compliant Limb Behavior = Grundmodelle Pedaler Lokomotion Basierend auf Nachgiebigem Beinverhalten. Ph.D. Thesis, Friedrich-Schiller-Universitat, Jena, Germany, 2005.
4. Seipel, J.; Kvalheim, M.; Revzen, S.; Sharbafi, M.A.; Seyfarth, A. *Conceptual Models of Legged Locomotion, in Bioinspired Legged Locomotion*; Elsevier: Amsterdam, The Netherlands, 2017; pp. 55–131.
5. Khan, A.T.; Li, S.; Zhou, X. Trajectory optimization of 5-link biped robot using beetle antennae search. *IEEE Trans. Circuits Syst. II Express Briefs* **2021**, *68*, 3276–3280. [CrossRef]
6. Xiang, Y.; Chung, H.-J.; Kim, J.H.; Bhatt, R.; Rahmatalla, S.; Yang, J.; Marler, T.; Arora, J.S.; Abdel-Malek, K. Predictive dynamics: An optimization-based novel approach for human motion simulation. *Struct. Multidiscip. Optim.* **2010**, *41*, 465–479. [CrossRef]
7. Gross, M.; Stevenson, P.; Charette, S.; Pyka, G.; Marcus, R. Effect of muscle strength and movement speed on the biomechanics of rising from a chair in healthy elderly and young women. *Gait Posture* **1998**, *8*, 175–185. [CrossRef] [PubMed]

8. Mak, M.K.; Hui-Chan, C.W. The speed of sit-to-stand can be modulated in Parkinson's disease. *Clin. Neurophysiol.* **2005**, *116*, 780–789. [CrossRef] [PubMed]
9. Odding, E. *Locomotor Disability in the Elderly: An Epidemiological Study of Its Occurrence and Determinants in a General Population of 55 Years and Over: The Rotterdam Study*; Erasmus University Rotterdam: Rotterdam, The Netherlands, 1994.
10. Janssen, W. *The Sit-to-Stand Movement Recovery after Stroke and Objective Assessment*; Optima Grafische Communicatie: Rotterdam, The Netherlands, 2008.
11. Janssen, W.G.; Bussmann, H.B.; Stam, H.J. Determinants of the sit-to-stand movement: A review. *Phys. Ther.* **2002**, *82*, 866–879. [CrossRef]
12. Anan, M.; Shinkoda, K.; Suzuki, K.; Yagi, M.; Ibara, T.; Kito, N. Do patients with knee osteoarthritis perform sit-to-stand motion efficiently? *Gait Posture* **2015**, *41*, 488–492. [CrossRef]
13. Rogers, M.W.; Chan, C.W. Motor planning is impaired in Parkinson's disease. *Brain Res.* **1988**, *438*, 271–276. [CrossRef]
14. Honda, K.; Sekiguchi, Y.; Sasaki, A.; Shimazaki, S.; Suzuki, R.; Suzuki, T.; Kanetaka, H.; Izumi, S.-I. Effects of seat height on whole-body movement and lower limb muscle power during sit-to-stand movements in young and older individuals. *J. Biomech.* **2021**, *129*, 110813. [CrossRef]
15. Hurley, S.T.; Rutherford, D.J.; Hubley-Kozey, C. The effect of age and seat height on sit-to-stand transfer biomechanics and muscle activation. *Phys. Occup. Ther. Geriatr.* **2016**, *34*, 169–185. [CrossRef]
16. Su, F.C.; Lai, K.; Hong, W. Rising from chair after total knee arthroplasty. *Clin. Biomech.* **1998**, *13*, 176–181. [CrossRef] [PubMed]
17. Yamada, T.; Demura, S.-I. Influence of the relative difference in chair seat height according to different lower thigh length on floor reaction force and lower-limb strength during sit-to-stand movement. *J. Physiol. Anthropol. Appl. Hum. Sci.* **2004**, *23*, 197–203. [CrossRef]
18. Yamasaki, H.R.; Kambara, H.; Koike, Y. Dynamic optimization of the sit-to-stand movement. *J. Appl. Biomech.* **2011**, *27*, 306–313. [CrossRef]
19. Garner, B. A Dynamic Musculoskeletal Computer Model for Rising from a Squatting or Sitting Position. Master's Thesis, The University of Texas at Austin, Austin, TX, USA, 1992.
20. Daigle, K.E. The Effect of Muscle Strength on the Coordination of Rising from a Chair in Minimum Time: Predictions of an Optimal Control Model. Master's Thesis, The University of Texas at Austin, Austin, TX, USA, 1994.
21. Domire, Z.J. A Biomechanical Analysis of Maximum Vertical Jumps and Sit to Stand. Ph.D. Thesis, The Pennsylvania State University, University Park, PA, USA, 2004.
22. Dodig, M. Models and modelling of dynamic moments of inertia of human body. *Int. J. Sport. Sci.* **2016**, *6*, 247–256.
23. Erdmann, W.S. Geometry and inertia of the human body-review of research. *Acta Bioeng. Biomech.* **1999**, *1*, 23–35.
24. Hall, S.J. *Basic Biomechanics, 8e*; McGraw-Hill: New York, NY, USA, 2019.
25. Williams, R. *Engineering Biomechanics of Human Motion*; Supplement Notes; Mechanical/Biomedical Engineering, Ohio University: Athens, OH, USA, 2014; p. 5670.
26. Ober-Blobaum, S.; Junge, O.; Marsden, J.E. Discrete mechanics and optimal control: An analysis. *ESAIM Control. Optim. Calc. Var.* **2011**, *17*, 322–352. [CrossRef]
27. Schultz, J.; Johnson, E.; Murphey, T.D. Trajectory optimization in discrete mechanics. In *Differential-Geometric Methods in Computational Multibody System Dynamics*; Springer International Publishing: Cham, Switzerland, 2015.
28. Inoue, Y.; Takahashi, M. Time-constrained Optimization of Sit-to-stand Movements in Contact with the Environment. *IFAC-PapersOnLine* **2022**, *55*, 358–363. [CrossRef]
29. Hirschfeld, H.; Thorsteinsdottir, M.; Olsson, E. Coordinated ground forces exerted by buttocks and feet are adequately programmed for weight transfer during sit-to-stand. *J. Neurophysiol.* **1999**, *82*, 3021–3029. [CrossRef]
30. Yamada, T.; Demura, S. The relationship of force output characteristics during a sit-to-stand movement with lower limb muscle mass and knee joint extension in the elderly. *Arch. Gerontol. Geriatr.* **2010**, *50*, e46–e50. [CrossRef]
31. Headon, R.; Curwen, R. Recognizing movements from the ground reaction force. In Proceedings of the 2001 Workshop on Perceptive User Interfaces, Orlando, FL, USA, 15–16 November 2001.
32. A Hanke, T.; Pai, Y.-C.; Rogers, M.W. Reliability of measurements of body center-of-mass momentum during sit-to-stand in healthy adults. *Phys. Ther.* **1995**, *75*, 105–113. [CrossRef]
33. Linden, D.W.V.; Brunt, D.; McCulloch, M.U. Variant and invariant characteristics of the sit-to-stand task in healthy elderly adults. *Arch. Phys. Med. Rehabil.* **1994**, *75*, 653–660. [CrossRef] [PubMed]
34. Bieryla, K.A.; Anderson, D.E.; Madigan, M.L. Estimations of relative effort during sit-to-stand increase when accounting for variations in maximum voluntary torque with joint angle and angular velocity. *J. Electromyogr. Kinesiol.* **2009**, *19*, 139–144. [CrossRef] [PubMed]
35. Wang, J.; Severin, A.C.; Siddicky, S.F.; Barnes, C.L.; Mannen, E.M. Effect of movement speed on lower and upper body biomechanics during sit-to-stand-to-sit transfers: Self-selected speed vs. fast imposed speed. *Hum. Mov. Sci.* **2021**, *77*, 102797. [CrossRef]
36. Lord, S.R.; Murray, S.M.; Chapman, K.; Munro, B.; Tiedemann, A. Sit-to-stand performance depends on sensation, speed, balance, and psychological status in addition to strength in older people. *J. Gerontol. Ser. A Biol. Sci. Med. Sci.* **2002**, *57*, M539–M543. [CrossRef] [PubMed]
37. Hughes, M.A.; Weiner, D.K.; Schenkman, M.L.; Long, R.M.; Studenski, S.A. Chair rise strategies in the elderly. *Clin. Biomech.* **1994**, *9*, 187–192. [CrossRef]
38. Schenkman, M.; Riley, P.; Pieper, C. Sit to stand from progressively lower seat heights—Alterations in angular velocity. *Clin. Biomech.* **1996**, *11*, 153–158. [CrossRef]

39. Weiner, D.K.; Long, R.; Hughes, M.A.; Chandler, J.; Studenski, S. When older adults face the chair-rise challenge: A study of chair height availability and height-modified chair-rise performance in the elderly. *J. Am. Geriatr. Soc.* **1993**, *41*, 6–10. [CrossRef]
40. Munro, B.J.; Steele, J.R.; Bashford, G.M.; Ryan, M.; Britten, N. A kinematic and kinetic analysis of the sit-to-stand transfer using an ejector chair: Implications for elderly rheumatoid arthritic patients. *J. Biomech.* **1997**, *31*, 263–271. [CrossRef]
41. Dempster, W.T. *Space Requirements of the Seated Operator, Geometrical, Kinematic, and Mechanical Aspects of the Body with Special Reference to the Limbs*; Michigan State Univ East Lansing: East Lansing, MI, USA, 1955.

Disclaimer/Publisher's Note: The statements, opinions and data contained in all publications are solely those of the individual author(s) and contributor(s) and not of MDPI and/or the editor(s). MDPI and/or the editor(s) disclaim responsibility for any injury to people or property resulting from any ideas, methods, instructions or products referred to in the content.